Aeolian processes as drivers of landform evolution at the South Pole of Mars

Isaac B. Smith [a,b,*], Aymeric Spiga [b], John W. Holt [c]

[a] Southwest Research Institute, 1050 Walnut St. #300, Boulder, CO 80302, USA
[b] Université Pierre et Marie Curie and Laboratoire de Météorologie Dynamique, LMD Boîte postale 99 Tour 45-55, 3e ét., Bur. 303A, 4 place Jussieu, 75252 Paris cedex 5, France
[c] University of Texas Institute for Geophysics, Jackson School of Geosciences, University of Texas at Austin, J.J. Pickle Research Campus, Bldg. 196, 10100 Burnet Rd. R2200, Austin, TX 78758-4445, USA

ARTICLE INFO

ABSTRACT

We combine observations of surface morphology, topography, subsurface stratigraphy, and near surface clouds with mesoscale simulations of south polar winds and temperature to investigate processes governing the evolution of spiral troughs on the South Pole of Mars. In general we find that the south polar troughs are cyclic steps that all formed during an erosional period, contrary to the troughs at the North Pole, which are constructional features. The Shallow Radar instrument (SHARAD) onboard Mars Reconnaissance Orbiter detects subsurface stratigraphy indicating relatively recent accumulation that occurred post trough formation in many locations. Using optical instruments, especially the Thermal Emission Imaging System (THEMIS), we find low altitude trough clouds in over 500 images spanning 6 Mars years. The locations of detected clouds correspond to where recent accumulation is detected by SHARAD, and offers clues about surface evolution. The clouds migrate by season, moving poleward from 71° S at ~L_s 200° until L_s 318°, when the last cloud is detected. Our atmospheric simulations find that the fastest winds on the pole are found roughly near the external boundary of the seasonal CO_2 ice cap. Thus, we find that the migration of clouds (and katabatic jumps) corresponds spatially to the retreat of the CO_2 seasonal ice as detected by Titus (2005) and that trough morphology, through recent accumulation, is integrally related to this seasonal retreat.

© 2014 Elsevier B.V. All rights reserved.

1. Introduction

Polar layered deposits (PLD) on Mars are primarily composed of water ice and dust (Grima et al., 2009; Fishbaugh et al., 2010; Hvidberg et al., 2012). The PLD together comprise the majority of surface ice on Mars, each rising above the surrounding terrain ~3 km, and are together comparable in volume to the Greenland ice sheet on Earth (Smith et al., 2001a). The north PLD (NPLD) and south PLD (SPLD) undergo seasonal variability, especially between winter (when CO_2 ice frost covers the polar regions) and summer (when the CO_2 ice has sublimed) (Kieffer et al., 2000; Kieffer and Titus, 2001; Byrne, 2009).

The surfaces of the PLD have enigmatic medium scale features, including chasmae larger than the grand canyon on Earth (Fishbaugh and Head, 2001; Farrell et al., 2008) and deep spiral depressions with 20–50 km wavelengths (Cutts, 1973; Howard et al., 1982; Smith et al., 2013) (Fig. 1). On the SPLD specifically, other features are found, including scallops with similar cross section to the spiral troughs but much smaller in breadth (Howard, 2000; Grima et al., 2011) and the aptly-named wirebrush terrain (Kolb and Tanaka, 2006). These features, resulting from erosional and depositional patterns of ice, are potentially

a key to understanding the history of the PLD and the water cycle on Mars.

Various processes have been invoked to explain observations associated with each PLD feature: basal melting (Clifford, 1987; Fishbaugh and Head, 2002), tectonics (Grima et al., 2011), viscous ice flow (Fisher, 1993, 2000), and brittle deformation (Murray et al., 2001), among others. Recent evidence on the NPLD has shown that the spiral troughs and Chasma Boreale likely formed within a constructional setting, with winds and atmospheric deposition likely playing the major roles (Holt et al., 2010; Smith and Holt, 2010; Smith et al., 2013). Observations of low altitude clouds and atmospheric modeling (Smith et al., 2013), surface morphology (Howard, 2000), in addition to radar stratigraphy (Smith and Holt, 2010) demonstrate that ice is transported across the NPLD by wind to form and modify these features; however, no studies have provided the same detailed combination of techniques to address the SPLD.

Here, we provide evidence that SPLD features, like those on the NPLD, are the result of persistent katabatic winds that contain katabatic jumps. In particular, we find that the SPLD spiral troughs belong to a set of morphological features called cyclic steps, which form because of fast winds and repeated katabatic jumps (Smith et al., 2013). Unlike on the NPLD, the SPLD troughs formed within a regime that has experienced more erosion than deposition, especially during the early stages. Our evidence includes topographic profiles, subsurface stratigraphy with

* Corresponding author at: Southwest Research Institute, 1050 Walnut St. #300, Boulder, CO 80302, USA.
E-mail address: Isaac@boulder.swri.edu (I.B. Smith).
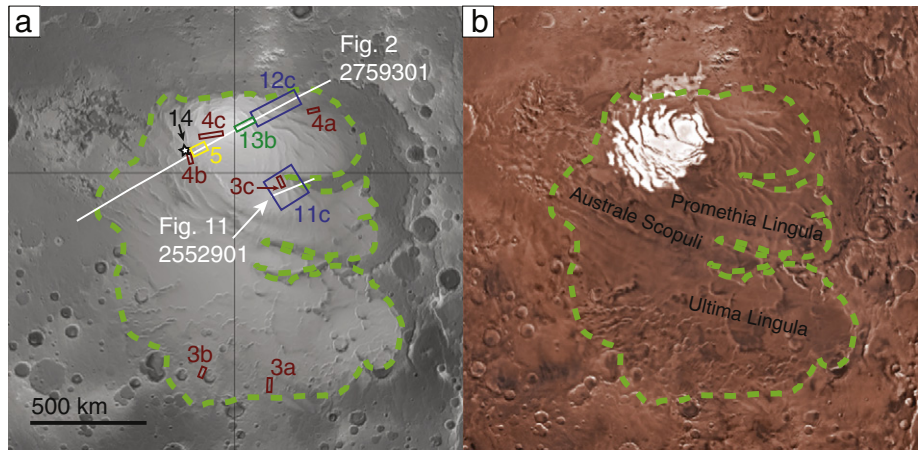
Fig. 1. SPLD surface and locations of the following figures. a) SPLD hillshade map. Ground tracks of SHARAD radargrams and footprints of optical imagery for future figures are listed with numbers. b) Viking color mosaic of SPLD with labeled geographic names. Residual CO_2 ice cap remains white through the Martian year, but the rest of the ice cap is covered by red dust in spring and summer. Large chasmae, spiral troughs, and scallops are visible. Green dashed lines delineate the approximate extent of the SPLD ice deposits.

the shallow radar instrument (SHARAD), and optical data that images the surface and atmospheric phenomena (i.e. clouds).

As a supplement to these observations, we employ a cap-wide high-resolution mesoscale atmospheric model on the SPLD. Global and regional (mesoscale) climate models have been developed for many years to predict circulation and clouds in the Martian atmosphere. In particular, NPLD features related to winds have been studied in detail (Massé et al., 2012; Brothers et al., 2013; Smith et al., 2013), yet few studies have attempted to relate the landforms on the SPLD to modeled winds (Koutnik et al., 2005).

As a reference we adopt a nomenclature of trough orientation based on elevation rather than one based on orientation. Trough high sides are always topographically higher than the low sides (Fig. 2). Descriptions based on orientation, such as "poleward" or "equatorward," are insufficient because troughs in some regions are oriented east-west, so these characterizations break down.

Furthermore, the terrain of each trough varies by location, so characterizations of morphology or stratigraphic exposure are fundamentally limited to the individual trough being examined. The high/low side topographic description has the advantage of being consistent across all troughs.

In Section 2 we provide a background for the rest of the paper. Section 3 introduces the methods utilized in this study, including optical observations detecting near surface clouds, radar observations of subsurface structure, and atmospheric modeling of surface temperature and near surface winds. In Section 4 we describe cloud detections, specifically spatial and temporal variability. Section 5 provides results of atmospheric simulations of an individual day and throughout the season. Modeled winds are compared temporally to cloud detections. In Section 6, we use SHARAD to associate the spatial detection of clouds with recent accumulation. Section 7 discusses these correlations and significance, and Section 8 provides some concluding remarks.
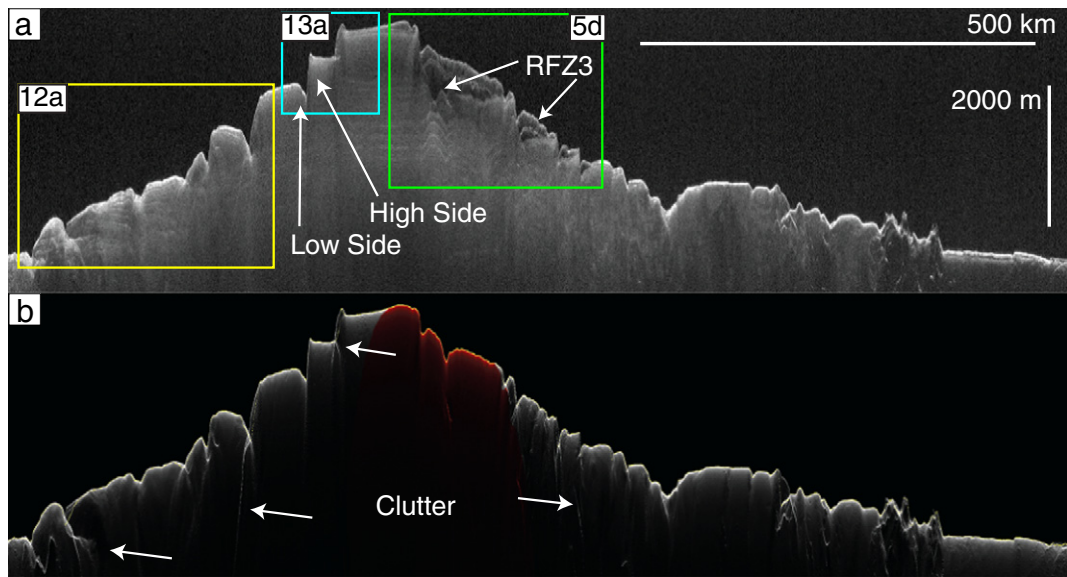
Fig. 2. SHARAD observation and clutter simulation 2579301. a) Troughs are topographically asymmetric. High side slopes generally face toward the equator and are always higher in elevation than low side slopes. Low side slopes generally face toward the pole. RFZ$_3$ unit has been interpreted as being massive CO_2 ice (Phillips et al., 2011). b) Clutter is from surface reflectors and provides no information about the subsurface. Boxes with numbers are later figures.

2. Background

2.1. Comparison of NPLD and SPLD

The north and south PLD have many similarities in composition and physical properties. For example, each cap rises about 3 km above the respective bases, and they are primarily composed of water ice (Grima et al., 2009; Fishbaugh et al., 2010; Hvidberg et al., 2012). They reach aerial extents of 1.12×10^{12} and 1.16×10^{12} km^2, respectively. The volumes of the NPLD and SPLD are on the same scale at 1.14×10^{15} and 1.20×10^{15} m^3 (Zuber et al., 1998; Smith et al., 2001a).

The PLD are similar in many ways, but they also have striking differences. Of primary importance are the basal elevations for each. The SPLD is found on the southern highlands, and its base is between 1 and 1.5 km above the average elevation of the planet, more than 6 km higher than the NPLD. The NPLD is located within Vastitas Borealis, the largest lowland on the planet ~5 km below the average elevation of Mars (Smith et al., 2001a). Even though the PLD encompass similar areas, the SPLD extends to ~ −71°, whereas the NPLD are generally all north of ~80°. Furthermore, the SPLD have a larger total topographic relief, being thicker by about 500 m. Atmospheric conditions, especially temperature and pressure, are strongly affected by these differences.

The interpreted ages of each pole are also distinct. Using crater counting statistics, the surface age of the uppermost NPLD has been determined to be less than 10^5 Earth years (EY) (Tanaka, 2005). Whereas the NPLD surface is relatively young, modeling evidence based on stability of ice at the North Pole found that the bulk of NPLD material must have been deposited within the last $\sim 4 \times 10^6$ EY (Levrard et al., 2007). The surface age of the SPLD has been dated to be $>10^7$ EY (Herkenhoff and Plaut, 2000), at least two times older than the majority of the NPLD. Thin surface deposits, however, may have covered smaller craters in some regions during the last 10^5–10^6 EY (Koutnik et al., 2002).

Another important distinction between the north and south PLD is that both poles experience a seasonal CO_2 ice frost, but only the SPLD retains a CO_2 ice cap throughout the year (Kieffer, 1979). The South Polar Residual Ice Cap (SRIC) contains <10 m thick CO_2 ice and represents a small portion to the entire cap. It retains its high albedo throughout the year (Fig. 1b) (Byrne and Ingersoll, 2003; Byrne, 2009). Furthermore, SHARAD detects large volumes of sequestered CO_2 ice filling in Australe Mensa troughs (RFZ$_3$ in Fig. 2) (Phillips et al., 2011), in contrast to the NPLD where no evidence of buried CO_2 ice has been found.

2.2. Processes on the poles

Recent studies have found that three observed processes are sufficient to explain all of the non-impact features on both poles: deposition, sublimation, and wind transport (Howard, 2000; Holt et al., 2010; Brothers et al., 2013; Smith et al., 2013). Atmospheric deposition is observed directly and indirectly. First, deposition is a necessary requirement of creating a deposit that contains alternating layers of ice and dust. Second, seasonal variations in albedo and elevation indicate that deposition and sublimation occur on an annual basis (Neugebauer et al., 1971; Farmer and Doms, 1979; Kieffer and Titus, 2001; Smith et al., 2001b).

Deposition of water ice from the atmosphere may come indirectly as snowfall (Whiteway et al., 2009) or directly as of frost. Locations with higher abundances of water vapor or that experience local cooling near the surface are the most likely to receive deposition. Sublimation occurs through several processes, primarily from increased temperatures during the day because of insolation and from thermal effects of winds on sloping terrains (Spiga et al., 2011).

Finally, wind transport of ice drives feature migration. On both PLDs, optical imagery provided evidence of ice transport in the form of wind streaks and erosion, in addition to morphologies and exposed layers postulated to be the result of migration (Howard et al., 1982;

Howard, 2000). SHARAD investigations detect subsurface stratigraphy that supported this interpretation for NPLD troughs (Smith and Holt, 2010).

2.3. Katabatic jumps and trough clouds

Low altitude clouds, called trough clouds because of spatial relationships with NPLD spiral troughs, are prevalent in spring and early summer for the SPLD (Figs. 3 and 4). Smith et al., 2013 interpreted them to be analogs to Antarctic clouds caused by katabatic jumps (Lied, 1964; Pettré and André, 1991), concluding that they are evidence for localized interactions between the atmosphere and surface.

Antarctic clouds are found at the site of katabatic jumps, or rapid changes in flow conditions of katabatic winds. A katabatic jump is described as "a narrow zone with large horizontal changes in wind speed, pressure, and temperature," (Pettré and André, 1991). Flow thickness often triples over a short distance, but wind velocities may decrease from as many as 20 ms^{-1} to as few as ~1 ms^{-1}. With sufficient water vapor, these strong perturbations, especially those associated with temperature decrease and pressure increase, are sufficient to explain the formation of clouds.

Smith et al. (2013) argued that Martian trough clouds form by the same processes as those on Earth and that these clouds are a mechanism of deposition on the low side of troughs. Evidence to support this claim came from terrestrial studies that found "walls of snow" beneath terrestrial clouds (Lied, 1964) (see Fig. 13 from Smith et al. (2013) or Fig. 2 from Pettré and André (1991)). If the clouds contribute to local deposition, they are an important part of understanding PLD surface morphology.

2.4. Cyclic steps

The three processes of wind transport, sublimation, and ice deposition at clouds are capable of explaining the stratigraphy and morphology that are observed at a single trough, but more was needed to understand the entire system of troughs. The cyclic step model provided the necessary mechanism. Cyclic steps are a distinct bedform that exists within "a train of upstream migrating bed undulations bounded by hydraulic [or katabatic for wind] jumps" (Parker, 1996; Kostic et al., 2010). Cyclic steps have been thoroughly studied on Earth, including those in erosional environments (Parker and Izumi, 2000) and depositional settings (Kostic et al., 2010). The spiral troughs of the NPLD belong to the depositional cyclic steps (Smith et al., 2013). Because cyclic steps repeat with a common wavelength (based on regional slope) and are created as a result of katabatic jumps, it is also likely that SPLD troughs also belong to this feature class.

2.5. Trough morphology and variety

Spiral troughs on the SPLD vary greatly from region to region and are often distinctly different from those on the NPLD. North polar studies have demonstrated that few or no troughs are purely erosional (Smith and Holt, 2010, in preparation), but the question of whether SPLD troughs are erosional or have migrated remains open.

The troughs on Promethei Lingula are primarily erosional features, with little evidence for migration (Kolb and Tanaka, 2001, 2006). In nearby Australe Sulci, where wirebrush terrain dominates, considerable evidence exists for erosion, including abrasive removal of material, supporting the eroded trough interpretation. Evidence does exist, however, for accumulation following trough incision. Kolb and Tanaka (2006) noted a thin lamination (Aa$_2$) on the low side of Promethei Lingula troughs (Fig. 5 from that paper). This lamination has covered or degraded craters smaller than 800 m in diameter, which skews crater counts toward larger craters (Koutnik et al., 2002). Evidence then supports the interpretation that the surface of Promethei Lingula is
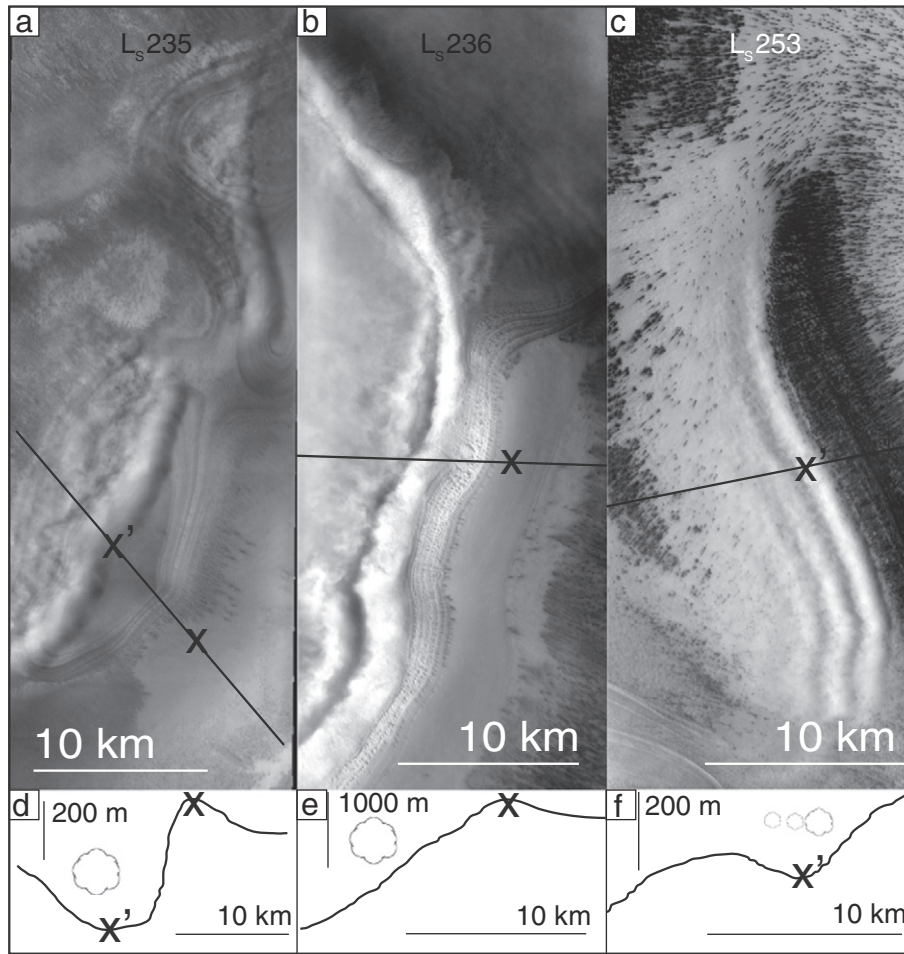
Fig. 3. THEMIS VIS images of trough clouds and cross-sectional topography. a) VIS image V07272010. Trough clouds are found just above the lowest portion of the troughs. b) VIS image V23982013. Cloud is found on high side slope, even though no slope break is present, demonstrating that changing topography is not a requirement for trough clouds to form. c) VIS image V15959007. Cloud has undular form and is found over lowest portion of trough. d), e) and f) are topographic profiles of a), b) and c). Topographic extrema are marked by X or X'. Cloud cartoons demonstrate the relative position of clouds with respect to the lowest portion of the trough. Cloud heights are only representative and not based on measurements. Image footprints in Fig. 1.

primarily made up of old erosional features with a small amount of recent accumulation.

Australe Lingula troughs are not as well studied as those of Promethei Lingula (Locations in Fig. 1b); however, they offer clues to atmospheric processes. Recent accumulation has been detected on trough low sides in this region, making them interesting targets for study (Fig. 9 of Byrne and Ivanov (2004)).

On Australe Mensa, at higher latitude and within the SPLD residual cap, troughs take on other forms and may be divided into two categories. Troughs spaced at regular intervals are readily visible from orbit, similar in scale to those on Australe Lingula (Fig. 1). Using SHARAD observations, Phillips et al. (2011) observed massive CO_2 ice that filled and partially buried these troughs. The second type of trough is much more shallow and closely spaced, located between the larger troughs. These troughs are only found at high latitudes and are unique to AA_3 (RFZ3 in Fig. 2) deposits within the residual cap (Figs. 4c, 5 and 3 from Phillips et al. (2011)).

2.6. Atmospheric modeling

Mesoscale atmospheric models have provided context for understanding wind patterns on the North Pole as a whole (Tyler and Barnes, 2005; Kauhanen et al., 2008; Spiga et al., 2011; Massé et al., 2012; Smith et al., 2013) and for understanding development of specific features on the north (Brothers et al., 2013) and South Poles (Koutnik

et al., 2005). These studies simulated the thermal properties of the atmosphere and, more relevant to troughs, the wind directions that affect geomorphic processes. When put into context of geologic features, wind vector maps tell of current processes near the surface, i.e. how winds respond to surface features. When put in context of the geologic record, atmospheric simulations are able to illuminate how ice and other volatiles are transported, i.e. how surface features respond to wind. Locally, mesoscale models may be designed with sufficiently high resolution to take into account medium scale topographic influences, including spiral troughs and scallops.

3. Methods

3.1. Optical imagery

As of this writing, more than 16,000 visible wavelength Thermal Emission Imaging System (THEMIS) images that capture portions of the SPLD are publically available (Christensen et al., 2004). We analyze the majority of these images to find near surface trough clouds. The SPLD is not symmetric about the South Pole, so regions of interest include the entire SPLD south of −80°, and between −80° and −71° for longitudes 90° to 220° (Fig. 6b). To supplement our THEMIS survey, we examine imagery from the High Resolution Stereo Camera (HRSC) (Neukum and Jaumann, 2004), Mars Orbital Camera (MOC) (Malin
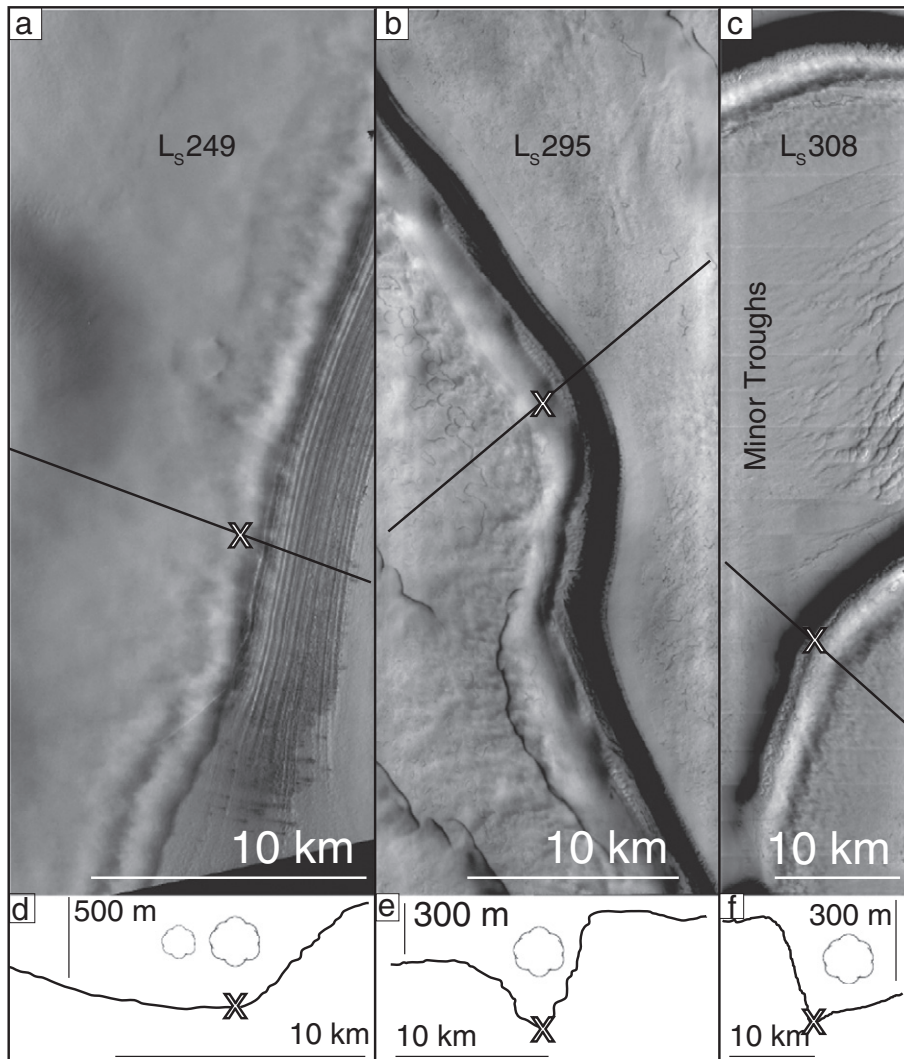
Fig. 4. THEMIS VIS images of trough clouds after mid-spring and cross-sectional topography. a) VIS image V15887005. Cloud has undular form and is found over lowest portion of trough. b) VIS image V41808006. Long cloud follows the lowest portion of trough. Swiss cheese terrain is found just downstream of this cloud. c) VIS image V08711007 in Australe Mensa. Trough clouds are found downstream of the local minimum elevation. Clouds are sites of katabatic jumps, where temperatures are lower – perhaps protecting the thin unit comprising the swiss cheese terrain. Optically thick clouds may also protect Swiss cheese terrain by reducing insolation. Minor troughs have high spatial frequency but very shallow cross sections. d), e) and f) are topographic profiles of a), b) and c). Topographic lows are marked by an X. Cloud cartoons demonstrate the relative position of clouds with respect to the lowest portion of the trough. Cloud heights are only representative and not based on measurements. Image footprints in Fig. 1.

et al., 1998), Context Imager (CTX) (Malin et al., 2007) and High Resolution Imaging Science Experiment (HiRISE) (McEwen et al., 2007).

Our survey is designed after the one conducted by Smith et al. (2013) for the NPLD, which examined every optical image of the NPLD in an effort to characterize low altitude clouds that interacted with the surface. They found nearly 400 images that capture clouds, ~350 from THEMIS and tens from other instruments. The majority of the clouds aligned parallel to spiral troughs (trough clouds). Here, we continue the search for clouds on the SPLD and implement some lessons learned in the northern survey. Our initial sampling included southern spring from L_s ~210° to ~280° (corresponding symmetrically to the NPLD cloud season) and was expanded to include dates from L_s 190° to L_s 330° for all of the SPLD. L_s is the angle of orbit around the sun, starting with L_s = 180° for southern vernal equinox.

To garner the best possible statistics, THEMIS VIS observations are examined from six Mars years: MY26 through MY31. Coverage varies by year, and SPLD observations decreased significantly after MY27 (Table 1). During the date range L_s 190°–320° MY27 had the most images with more than 4600. MY26 had ~4000 for the same range. By MY28, fewer than 1700 images were taken in that period. MY29–MY31 had ~850, ~470, and ~550, respectively. Furthermore,

MY29, MY30, and MY31 campaigns were limited to a few targets, reducing coverage. The MOC wide angle camera detects trough clouds as early as MY25 in the same date range.

3.2. Radar observations

SHARAD has been operating since late 2006 and has collected approximately 11,500 observations of Mars. The abundance of observations, especially near the South Pole, is useful for analysis. The instrument sends a chirped pulse between 15 and 25 MHz (at a rate of 700 pulses per second) to detect subsurface contrasts in permittivity with a vertical resolution of about 15 m in free space and 8.4 m in ice. Multiple pulses are coherently summed onboard MRO. After relay to Earth, pulse compression, synthetic aperture focusing, and corrections for ionospheric distortion are performed (Campbell et al., 2011). After processing, SHARAD resolves targets down to 0.3–1 km along track and 3–6 km cross track (Seu et al., 2007b).

Occasionally, we utilize repeated and crossing observations to increase confidence in interpretations. Repeated observations are important for checking against artifacts of processing or low signal strength, which may hamper an individual observation. Crossing
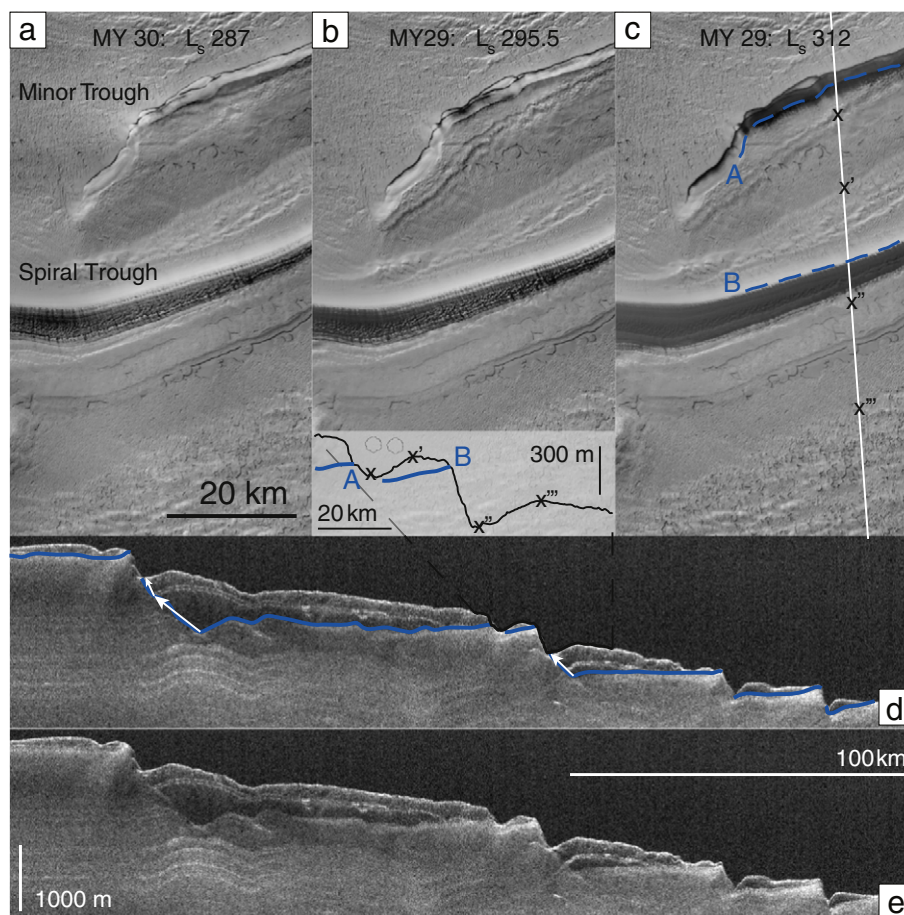
Fig. 5. Observations in Australe Mensa. a) CTX image G11_022371_0932_XI_86S057W at L_s 287 showing minor and major troughs, localized Swiss cheese terrain, and trough clouds. b) CTX image B11_013734_0932_XI_86S057W, similar to a) but at L_s 295.5. c) CTX image B11_014090_0932_XI_86S057W at L_s 312. In each image undular clouds are found at the minor troughs (changing slightly between dates) but not at the major trough. Seasonal frost is reduced on trough high sides as the season progresses. Contact of overlying RFZ_3 and underlying water ice is shown with blue dashed line. White line in c) corresponds to ground track of inset and d), and inset is blow up of interpretation from d). d) Portion of radargram 2579301. RFZ_3 is distinct from lower water-ice deposits (contact in solid blue line). Troughs were filled in during deposition of CO_2 ice and have migrated 10s of kms during a small amount of accumulation (white arrows). e) Uninterpreted radargram 2579301.

observations are important for eliminating ambiguous interpretations. Furthermore, multiple observations of a target help to separate side reflections, or reflections from targets other than the one of interest, from scientifically interesting subsurface reflections. Because side reflections received by SHARAD often have an undesirable nature, they are considered "clutter".

Clutter cannot be removed from a radargram, but it can be mitigated. We compare SHARAD observations to clutter predicted from surface topography (Smith et al., 2001a) to determine which part of the signal comes from the subsurface (Fig. 2b) (Holt et al., 2006). A synthetic radargram only predicts what reflections the instrument will receive from the surface; thus, echoes in the actual radargram that are not present in the cluttergram are considered as arising from the subsurface. We employ clutter mitigation techniques in our analysis and present radargrams that are favorable for interpretation.

Radar data are recorded in time. Our interpretations are done in this native format, to reduce uncertainties. To display more accurate geometry in this paper, we convert time-delay radargrams to depth by assuming a dielectric constant, ε, which determines wave velocity. We assume ε for a composition of water ice, 3.15, consistent with the value determined for the NPLD (Grima et al., 2009) and previous SPLD radar investigations (Plaut et al., 2007; Seu et al., 2007a; Phillips et al., 2011). Modifying this value, would only affect the depths measured by a few percent.

3.3. Atmospheric modeling

To simulate atmospheric conditions on the SPLD, we use a mesoscale model developed at the Laboratoire de Meterologie Dynamique (LMD) (Spiga and Forget, 2009) based on the Weather Research and Forecast model (Skamarock and Klemp, 2008). Our SPLD simulations are comparable to those that have been conducted on the NPLD (Spiga et al., 2011; Massé et al., 2012; Smith et al., 2013). Several aspects are simulated: wind speed and direction, and surface temperature. Hourly results are output for an equally divided "24-hour" Mars day (Fig. 7). We simulate the conditions at several dates throughout spring and summer, including L_s 230°, 260°, 290°, and 330° (Fig. 8).

To model near-surface winds, it is particularly important to account for the evolution of the seasonal CO_2 ice deposit. As was shown through mesoscale modeling by Siili et al. (1999) and Toigo et al. (2002), near-surface regional winds over Martian polar caps are controlled by topography and surface temperature, hence CO_2 ice deposits, which fix the surface temperature to below 150 K (Fig. 8t1). Our mesoscale simulations, therefore, use a prescribed CO_2 seasonal deposit that evolves by L_s date according to infrared measurements of the surface temperature during three Mars years (24, 25, and 26) (Titus, 2005). We use the analytical functions provided by that study to obtain the crocus line, i.e. the external boundary of seasonal CO_2 ice deposits (named after a crocus flower that blooms as ice recedes (Kieffer et al., 2000)).
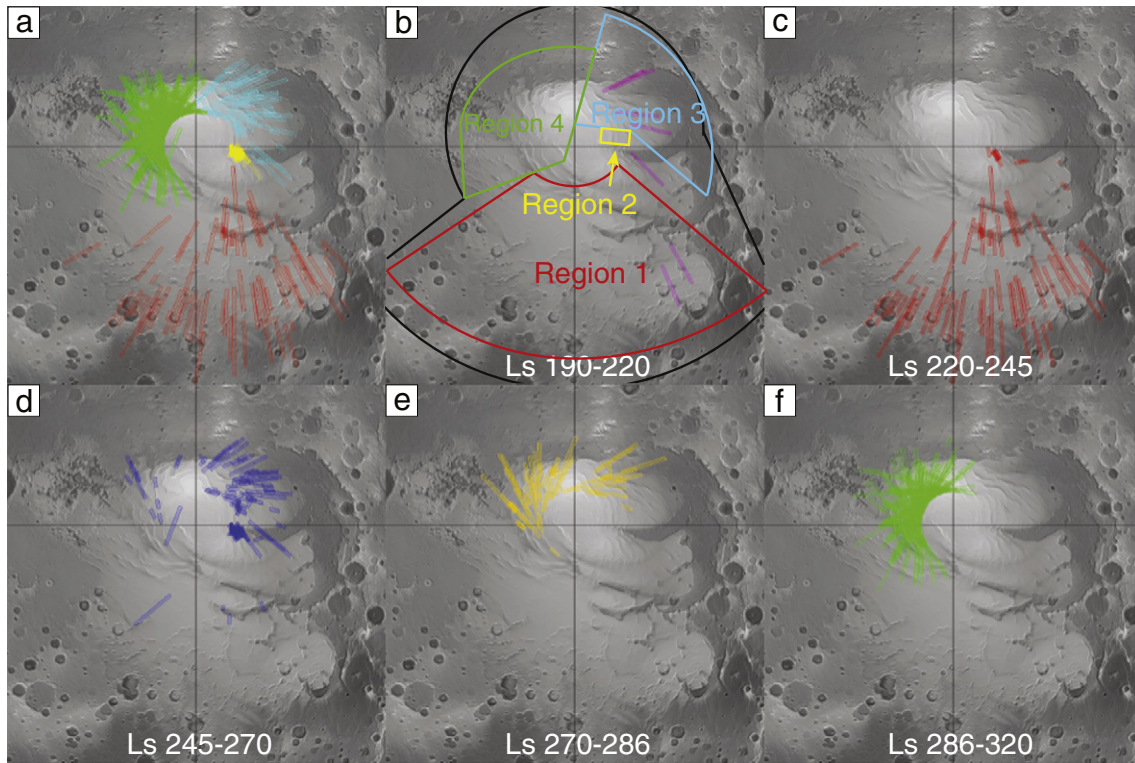
Fig. 6. SPLD basemaps showing footprints of THEMIS cloud detections and poleward progression in spring and summer. a) Cloud detections in all regions (color coded with Fig. 9). b) Clouds detected between L_s 190° and L_s 220° in purple. Regions 1 through 4 are color coded and outlined. Black lines outline the total area surveyed for trough clouds. c)–f) Clouds detected between L_s 220° and L_s 245° in red; L_s 245°–L_s 270° in blue; L_s 270°–L_s 286° in orange; L_s 286°–L_s 320° in green. No clouds are found outside of Regions 1 and 2 after L_s 245°, nor are clouds detected outside of Region 4 after to L_s 286°. The four regions are distinct based on timing and location of clouds.

Our simulations cover the entire SPLD and surrounding regions: ~1800 km by 1800 km centered on 86° south and 173° east. The grid is 101 by 101 cells, yielding a resolution of ~18 km per cell. At this resolution the large chasmae and general topography of the SPLD are represented, but smaller features are not present. Because the intent of this initial study is to focus on regional wind patterns and variations on the seasonal and diurnal scales, our simulations are adequate. With the goal of understanding local effects of topography on the atmosphere, future work will focus on individual features.

4. Observations of SPLD clouds

Trough clouds are detected over large ranges of latitude, elevation, and date (Figs. 3, 4, 6 and 8). Spatially, trough clouds are found at all latitudes of the SPLD, from −71° to 89°S. They manifest near topographic changes, especially where slopes decrease (near the bottom of troughs).

Table 1
Count of THEMIS images for seven Mars years: total images analyzed, images in cloudy season, images containing clouds, percentage of images that contain clouds in the cloudy season. Cloudy seasons in MY 26 may have been an extreme year. High percentage in MY 30 is likely due to biasing. Clouds are most abundant in Region 4 where targeting was concentrated.

Mars year	Total images	Ls 190–320	Trough clouds	Percentage in Ls 190–320
25	31	0	0	0.0
26	5284	3983	217	5.4
27	6887	4658	155	3.3
28	2337	1669	29	1.7
29	1087	853	15	1.8
30	551	475	30	6.3
31	787	552	17	3.1
	16,933	12,190	463	

Corresponding to the symmetric season of observed clouds on the NPLD, many SPLD clouds are found from mid-spring until early summer. This encompasses L_s range 220°–280°. SPLD trough clouds, however, are observed earlier and later than NPLD counterparts, and four clouds are detected prior to L_s 210°, as early as L_s 198 (Fig. 9). Quite unexpectedly, trough clouds are observed until L_s 318, much later than the corresponding NPLD date (Figs. 6 and 9). The total seasonal range for south polar trough clouds is ~120° L_s, far greater than the ~60° of L_s on the NPLD (Smith et al., 2013).

Besides the addition of a second, later season, trough clouds are detected at locations that vary spatially in correspondence to date (Figs. 6 and 8m1–m4). We divide the SPLD into four regions based loosely on the timing of detected clouds and latitude and elevation (Fig. 6b). In general, clouds at lower latitudes occur earlier in the spring, and clouds of higher latitudes appear later. Based on THEMIS images, Regions 1 through 4 each contains 80, 64, 89, and 230 observed clouds, respectively.

Region 1 corresponds to Ultimi Lingula, between 120° and 235° E and 70°–83.5° S (Figs. 1b and 6b). 80 trough clouds are found in this region between L_s 210° and 254° for a total duration of 44° of L_s (Fig. 3a and b). The bulk of detections (74) are between L_s 229° and 245°. Only 4 images capture clouds in Region 1 after L_s 245°, so this region sees the most activity in the early part of the cloudy season (Figs. 6c and 9).

Region 2 is much smaller than the other regions. It resides from 85° to 110°E and 85.5° to 87°S and is distinguished by its location at the head of Chasma Australe (Fig. 6b). This small region was heavily targeted by THEMIS, allowing for more observations throughout the Mars years. More than 60 clouds are detected there, spanning from L_s 225° through 268° (Figs. 3c and 6c, d). Prior to L_s 243° only five clouds are detected in Region 2, so a more concise range is L_s 243°–268°, or about 25°. Region 2 clouds occur during a transition period between Regions 1 and 3 (Fig. 9).
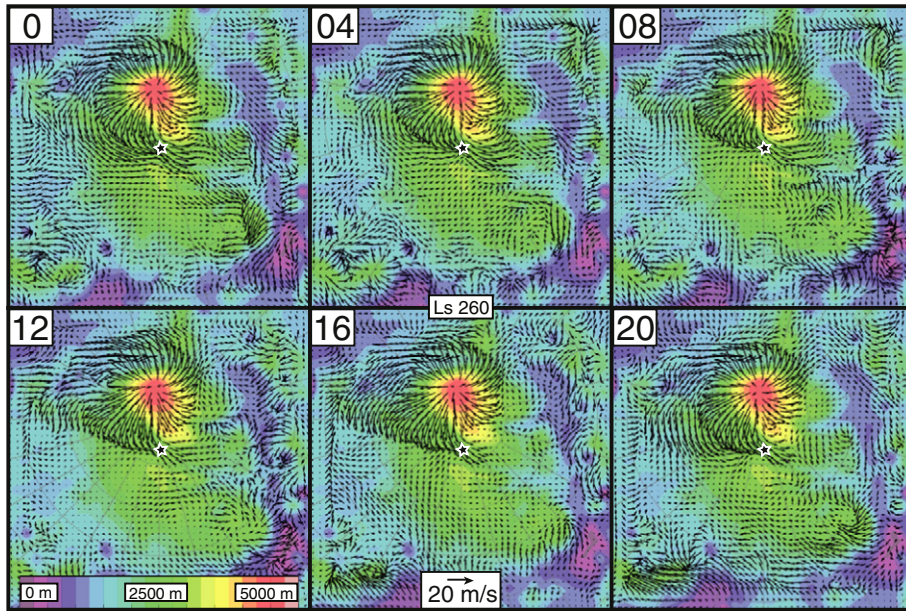
Fig. 7. LMD mesoscale simulations at L_s 260° of wind speed and direction 20 m above the surface. Each panel represents winds at 0° E longitude local time (0–20 h) overlaying colorized terrain. Winds exhibit a diurnal cycle in intensity. Fastest winds are found within and just outside of the crocus line (the extent of the CO_2 seasonal cap as seen in Fig. 8). At this date fast winds are funneled near the wirebrush terrain (at star) throughout the entire day and parallel to erosional scours.

Region 3 experiences trough clouds over a longer duration than other regions. It resides at a higher latitude than Region 1, between 80° and 86.5°S and extends over an enormous elevation range (~3500 m). Longitudinally, Region 3 spans 5° to 110°E (excluding Region 2). The majority of Region 3 clouds are observed between L_s 241° and 295°, for a duration of 54° (Figs. 9 and 4a). The earliest detected clouds on the SPLD are here: L_s 198° through 228°. No clouds are detected from L_s 228° to 241°.

Finally, Region 4 primarily contains Australe Mensa and the residual CO_2 ice cap but extends to the margin near 83° (Fig. 6b). All detections of trough clouds after L_s 286° are found in Region 4, for a total of 173 images (Figs. 4a, b, 5, 6f, and 9). The remaining 60 detections are as early as L_s 250°, with 55 between L_s 265° and 286°. During the earliest part of Region 4's window of detection, L_s range 250° to 265°, only 5 clouds are imaged. Those 5 events are found nearer to the margin than the other clouds and appear to be isolated. The majority of Region 4 trough clouds are at high latitudes and between L_s 265° and 318°, the last date of observed clouds on the SPLD.

The four regions were delineated based on timing and location, but some regions exist in which no clouds are observed, including a dearth of detections in Promethei Lingula (except near the head of Chasma Australe) and Australe Scopuli. This reinforces the observation of strong local control on frequency and timing of cloud formation. Furthermore, no trough clouds are found in the vast, smooth plains between Australe Mensa and Ultimi Lingula. Coverage in these regions is comparable to those where clouds are detected, so sampling density is an unlikely explanation (Fig. 8m1–m4). Additionally, THEMIS and other optical instruments have poor coverage south of ~88°, due to orbital inclination, inhibiting detection there.

A southward progression of detected clouds is observed (Figs. 6 and 8m1–m4). Between date ranges L_s 220° and 230° all but one cloud is found in Region 1. Between L_s 250° and 257° no clouds are detected in Region 1, but many are found in Regions 2 and 3. During this period Region 4 has few detections, primarily at the SPLD margin. Between L_s 280° and 300°, the majority of clouds are in Region 4, with only a few in Region 3. Eventually, after L_s 320°, no clouds are detected.

Spatial coverage is robust, but THEMIS coverage of the SPLD varies greatly by year. Because of that, our statistics will not be as solid as they were for the NPLD, where coverage was more even. Nevertheless,

we have analyzed thousands of THEMIS images and hundreds from other instruments and are confident that the four regions are distinct and that the clouds follow a southward progression throughout the year.

## 5. Simulated winds spatially related to trough clouds

Using mesoscale simulations described in Section 3.3, we map surface temperature and wind vectors 20 m above the SPLD surface. Fig. 7 shows that near-surface winds undergo a moderate daily cycle, so that we focus our analysis on comparing winds at various seasons for a fixed local time, 23 h (Fig. 8).

On a seasonal basis, it appears that the location of the crocus line has a strong impact on surface wind speeds, and the fastest winds on the SPLD are often found in the vicinity of this line. As the season progresses and the seasonal cap retreats toward the pole, so do the fastest winds (Fig. 8t1–t4), consistent with the mesoscale simulations of Toigo et al. (2002), who found that the cap-edge thermal contrast yielded high surface wind stresses likely to give birth to high dust storm activity (Cantor et al., 2001).

The physical mechanism for thermal circulations is well known on Earth with "sea-breeze" circulations. Thermal surface heterogeneities in a given region (e.g. sea vs. continent on Earth; ground CO_2 ice vs. bare soil on Mars) lead to regional temperature gradients. Through hydrostatic equilibrium, this in turn leads to regional pressure gradients. Thermally-direct circulations arise (Fig. 10b), with a possible deflection by the Coriolis force if the atmospheric motions extend from regional to planetary scales.

As it was described by Siili et al. (1999) through idealized simulations, the SPLD regional circulation in the vicinity of the crocus line boundary likely results from a combination of cap-edge circulations and slope winds. This is confirmed by our mesoscale simulations. The topographical heights of the SPLD primarily drives slope-wind (katabatic) circulations, as is the case for most regions on Mars featuring uneven topography, e.g. Spiga et al. (2011). This existing circulation is reinforced by an additional thermally-direct circulation analogous to the sea-breeze circulation on Earth. The combination of those two kinds of regional circulations in driving the near-surface winds is expressed in Fig. 8 and summarized by the schematic Fig. 10, explaining why
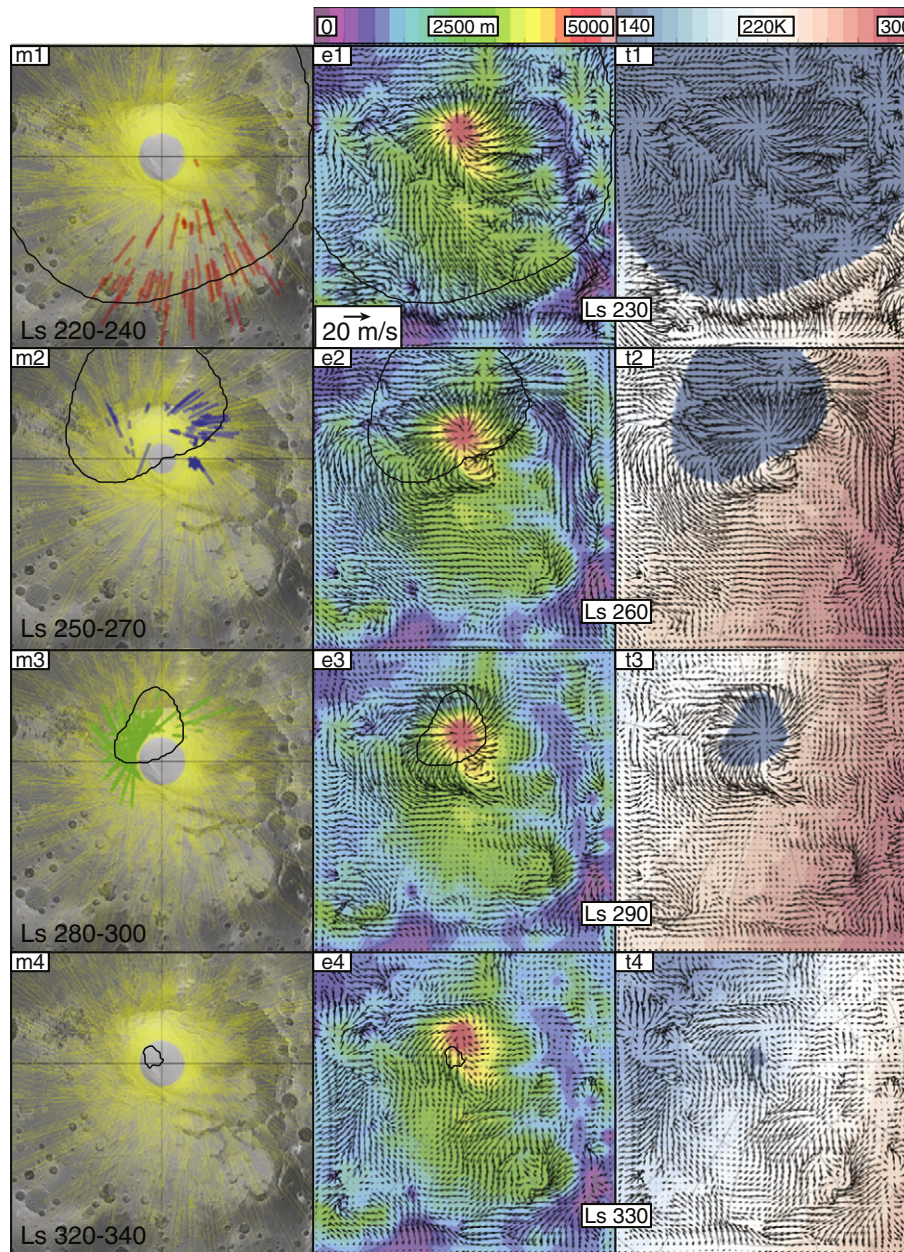
Fig. 8. Maps of SPLD for cloud detections, wind speeds corresponding to topography and temperature. m1–m4: Cloud detections (in red, blue, and green) overlaying available THEMIS image footprints (yellow). For these date ranges, a plethora of observations are available (yellow), and detections of clouds are not limited by spatial coverage. A strong poleward progression of cloud is detected as time of year increases. Solid black line corresponds to the crocus line, or line of CO_2 seasonal ice extent. e1–e4: Map of SPLD wind vectors 20 m above the surface overlying colorized topography. Winds generally have higher velocities near strong slopes. t1–t4: Map of SPLD wind vectors 20 m above the surface and surface temperature. As the season progresses (L_s 230°, 260°, 290°, and 330°) CO_2 seasonal ice retreats (seen in blue with surface temperature ~150 K) (Titus, 2005). The highest wind speeds on the pole are found near the greatest temperature contrast, at the crocus line. Basemap same as Fig. 1a.

enhanced winds are mostly found in the vicinity of the crocus line, but not necessarily at the precise location of this line.

The simulation for L_s 290° is maybe the most illustrative example of this combination (Fig. 8t3). The crocus line is located so that the slope winds produced by the SPLD topographical summit is optimally enhanced by thermally-direct circulations caused by the nearly 100 K contrast between surface temperature above the CO_2 seasonal cap and the lower-latitude dusty terrains. Near-surface winds can reach speeds approaching 20 ms^{-1}. Later in the season, at L_s 320°, the temperatures outside the crocus line are cool enough that the cap-edge thermal contrast is significantly reduced, causing no near-surface winds to be predicted above 10 ms^{-1} in the model.

A comparison of trough cloud locations with measured seasonal cap retreat shows a strong spatial correlation (Fig. 8m1–m4). Clouds retreat at about the same rate as the crocus line. Furthermore, our simulations agree that strong winds, enhanced by thermal contrasts and slopes, are near the sites of cloud detections.

This scenario is supported in most cases, shown in Fig. 8, but the relationship between strong winds and trough clouds is less clear at L_s 230°. Near Australe Mensa the modeled winds are extremely fast and divergent from the pole, but no trough clouds are detected. This reminds us that strong winds conducive to the formation of katabatic jumps are a necessary but not sufficient condition for trough clouds. Those clouds need the water vapor mixing ratio in the atmosphere to
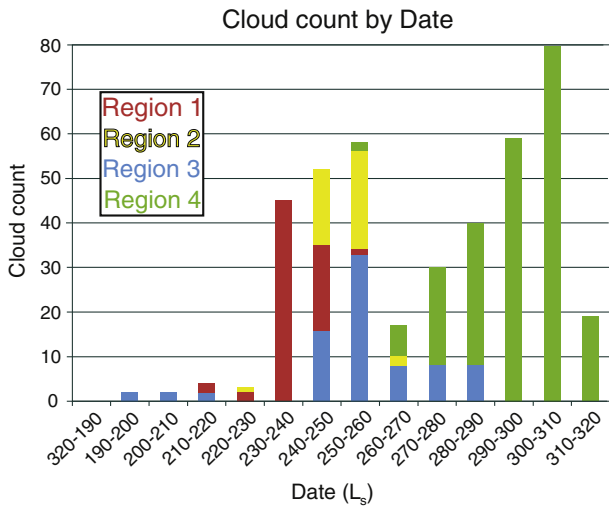
Cloud count by Date

be high enough to form. It is very likely that the cold trap of ground water ice by seasonal CO_2 ice (e.g. Montmessin et al., 2004) is very effective on Australe Mensa at L_s 230°, which would account for low water vapor mixing ratios in the atmosphere and consequent lack of cloud detection.

Another point for consideration is that katabatic winds enhance sublimation on trough high sides, removing CO_2 ice and exposing the underlying water ice there earlier. This exposure provides some of the required water vapor necessary to form clouds at troughs detected within the crocus line.
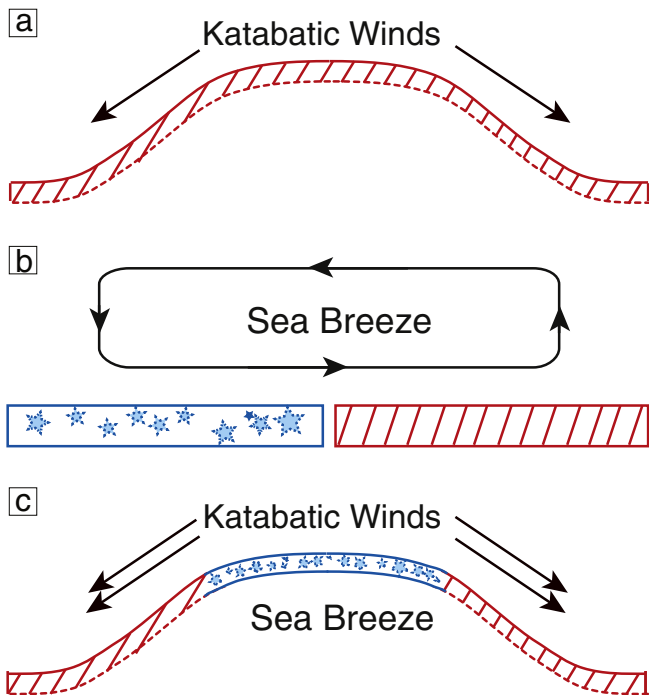
Fig. 10. Cartoon depiction of topographic and temperature forcing on polar winds. a) Katabatic (slope) winds form because of pressure gradients set up by radiational cooling of the lower atmosphere. b) Thermal contrasts between seasonal CO_2 ice (<150 K) and exposed soil (as much as 300 K seen in Fig. 8t) set up a common "sea breeze" circulation. c) At some dates, a combination of slope winds and strong temperature gradient reinforce the winds, and velocities as high as 20 ms^{-1} can be attained (Fig. 8).

These simulations are not employed with the very high spatial resolution necessary to resolve individual troughs or the katabatic jumps that take place within those troughs. Because of this we cannot predict clouds in our model. Predicting individual clouds requires dedicated and unprecedented modeling that we leave for future work.

6. Trough observations

We find that the locations of trough clouds are good predictors for where recent accumulation has occurred. In particular, SHARAD detects shallow subsurface layering on many low side slopes in regions where clouds are found. Where clouds are not found, e.g. over the majority of Promethei Lingula, SHARAD does not detect such layering. In Region 4, where clouds are abundant, large amounts of ice have filled the troughs. Intermediate volumes of ice are found in Australe Lingula, where clouds are present but are not detected as frequently as in Australe Mensa.

6.1. Promethei Lingula

The troughs of Promethei Lingula are broad and symmetric. They have wide cross sections, and relatively shallow depths (Fig. 11). Those at lower latitudes, nearest Chasma Australe, have decreased low-side slopes. This overall symmetry makes Promethei Lingula troughs distinct from other regions. In optical imagery, these troughs display clear evidence of outcropped layering on the trough high sides (exposed layers I and X in Fig. 11c), but the trough low sides only
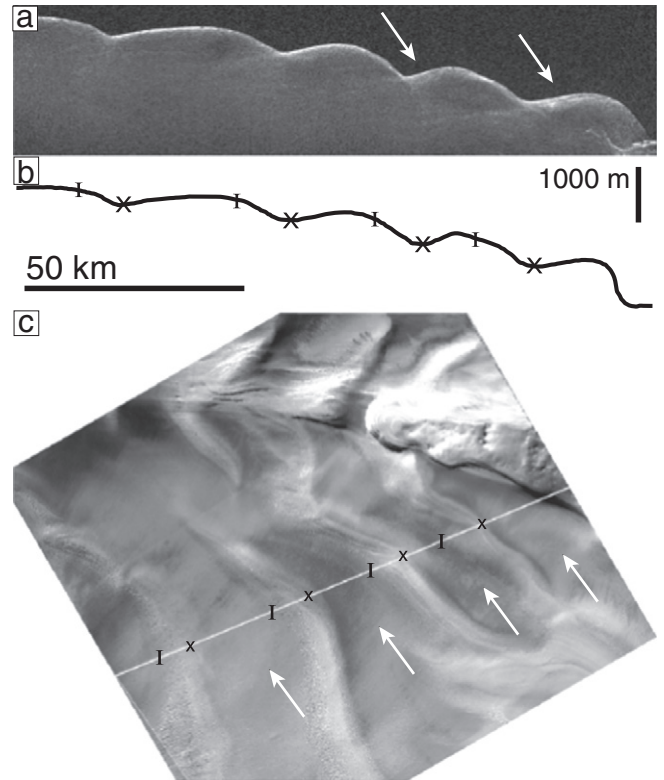
Fig. 11. Observations of Promethei Lingula. a) Radargram 2552901. Troughs are broad and more symmetric than in other regions (including the NPLD). Internal reflectors showing subhorizontal layering are very faint and demonstrate that troughs were eroded into existing deposits. Low side accumulation is minimal on the lowest two troughs (arrows) indicating that relatively little recent accumulation has occurred. b) Topographic profile of ground track in c). X marks the lowest points within a trough. I's mark where layers are exposed on the trough high side. c) HRSC image H2286_0000_ND3 showing surface exposure on Promethei Lingula. Trough high sides have exposed layers (I), but low sides are smooth without layers. Some wind streaks are visible on low sides. A thin deposit covers the trough high sides (arrows) (Koutnik et al., 2002).

show some wind streaking. Neither layers nor banded terrain (as on the NPLD) are visible on the low sides.

The combination of reduced slopes and lack of layering on the trough low sides indicates some accumulation after the troughs formed. Furthermore, SHARAD detects conformable layering of ~50 m on the low side of the lowest two troughs, indicative of recent deposition. Where reflections are visible in the radar (white arrows in Fig. 11a) a hint that the troughs have migrated slightly toward the high side exists. These observations are in agreement with the detection of a thin deposit, Aa_2, onlapping the low side of the troughs (Koutnik et al., 2002; Kolb and Tanaka, 2006).

6.2. Australe Lingula

At latitudes equatorward of ~86° S in Australe Lingula, layered outcrops common to all troughs are exposed on trough high sides (red in Fig. 12). Meanwhile, low sides expose no layers. Radar reflections on the low sides and inter-trough regions are conformal to deeper eroded surfaces, separating recent deposition from the erosion of the spiral troughs at an angular unconformity (blue in Fig. 12a). Accumulation is much thicker than in Promethei Lingula, ~140 m. This is most clear at the lowest latitudes, where the thickness of the upper section is greatest between troughs and reduces as it approaches the high or low sides of adjacent troughs. This contrasts with the NPLD, where thicknesses are generally greatest at the trough low side (Smith and Holt, 2010). Accumulation on the low side points to poleward migration, albeit reduced from north polar observations. Higher latitude troughs are also described in the same way, but the troughs are deeper and increasingly asymmetric.

The two highest troughs on Australe Lingula are quite distinct (Fig. 13a). In some locations, these troughs have sub-horizontal low sides and steep high sides, giving them highly asymmetric, step-like cross sections. Even with these irregularities, these troughs have similarities to other major troughs on the SPLD: layered terrain is exhibited on the high side and no layers are exposed on the low side (Figs. 13b and 9 from Byrne and Ivanov (2004)). SHARAD agrees with this interpretation and detects reflectors that intersect the trough high side and extend into the next trough's low side (X' to X"). Little variation in thickness is detected, suggesting minimal wind transport since this material was deposited (Fig. 13a).

Another contributing factor to the asymmetry of these highest troughs is a pair of high side ridges, or raised edges (Fig. 13a) (Howard, 2000). Unlike troughs on the NPLD and in nearby locations on the SPLD, the high sides of these troughs are raised more than 50 m above the surrounding terrain, immediately above the high side slope.

6.3. Residual cap troughs

SRIC troughs offer more variety to the already complex SPLD trough system and have characteristics all-together different from those discussed previously. We find two distinct types of troughs on the SRIC: major asymmetric troughs, within the Bench Forming Layer (described by Milkovich and Plaut (2008); and minor troughs, within the AA_3 sequence (Fig. 4c, 5a and 3 from Phillips et al. (2011)).

Topographically, minor troughs are much smaller in wavelength, extent, depth, and breadth than any other troughs on the SPLD. Where elevation data are available, minor troughs range from ~10 m–>100 m deep, but only a few are at the high end of that range (Figs. 4b and 5a). Because these troughs are smaller in size, they have a much higher spatial frequency. Between 5 and 20 minor troughs may be found between two major troughs. SHARAD detects some of the minor troughs, albeit only the largest amplitudes are greater than the resolution of the radar (Fig. 5b inset and 5d). Minor troughs exhibit neither the traditional layering nor banded terrains in optical imagery.

Evidence from SHARAD has shown that the low sides of Australe Mensa major troughs are filled with up to 700 m of CO_2 ice (Phillips et al., 2011). The former topography of these troughs can be detected and mapped with SHARAD (blue in Fig. 5d), revealing that the
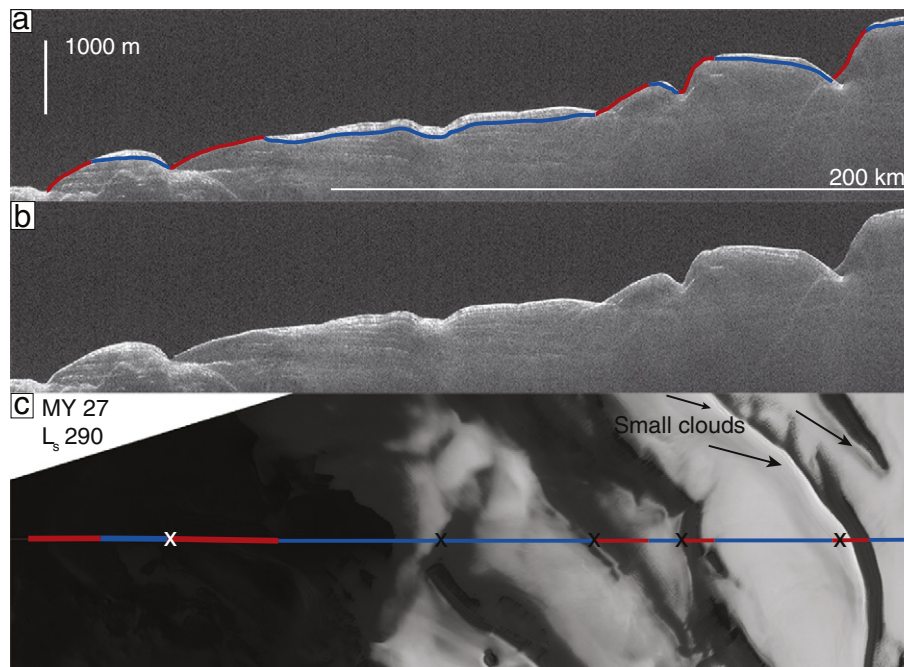
Fig. 12. Observations of troughs in Australe Lingula. a) and b) Portion of radargram 2579301. Trough high sides (red) show no evidence of recent accumulation. Trough low sides and inter-trough regions (blue) have >100 m of accumulation post trough formation. An angular unconformity separates the youngest section from underlying deposits (F from Byrne and Ivanov (2004)). Lower section corresponds to Promethei Lingula Layers from Milkovich and Plaut (2008). Northernmost troughs (left) are more symmetric than more southern troughs (right). This represents the transition from Promethei Lingula Layers to Bench Forming Layers. c) HRSC image H2155_0000_ND3. Surface exposures of layers correspond to where SHARAD does not detect recent accumulation (red). Locations without exposed layers correspond well to where SHARAD detects accumulation (blue). Horizontal line is ground track for a), and Xs mark local topographic minima. Two sets of clouds appear in the northernmost troughs.
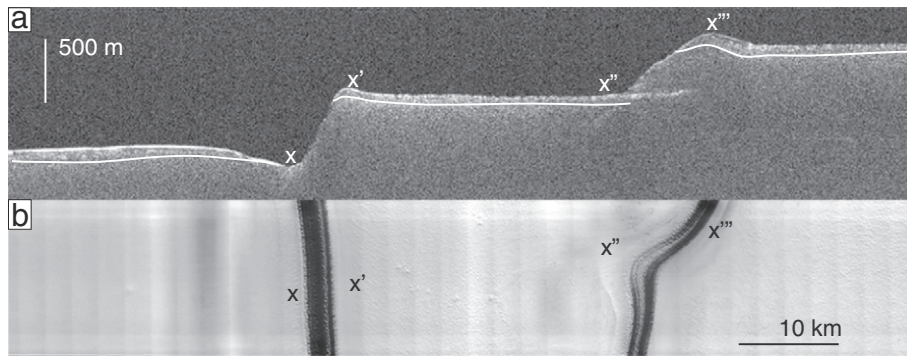
Fig. 13. Observations of asymmetric troughs in Australe Mensa. This region corresponds to the Bench Forming Layers, which gives these troughs a stair-step like cross section (also observed in Fig. 5d) (Milkovich and Plaut, 2008). a) Portion of radargram 2579301 showing weak reflectors that detail recent accumulation corresponding to low side deposits. Presence of ridges on the troughs high side remains an enigma (Howard, 2000). b) THEMIS image V16611013. High side layers expose water ice, while low sides are smooth. Black line is ground track in a).

cross sections of these troughs have been modified from their original, erosional morphology. Previously, the major troughs were very asymmetric with steep high sides and relatively shallow low sides, similar to the morphologies of the troughs of Australe Mensa (Fig. 13).

After infill, the troughs are topographically more symmetric than in a previous state (Fig. 5d). Strong asymmetry in the exposures and in radar, however, remain on each side of these troughs (Fig. 5c). The trough high sides have low albedo and layered outcrops corresponding to water ice. Low sides, on the other hand, have a high albedo and many sublimation features, including pits and Swiss cheese terrain (Figs. 4b and 5c). SHARAD demonstrates that low sides are part of the RFZ_3 unit. No other troughs on Mars have such a strong asymmetry in composition.

Adding to the complexity, some SRIC troughs may be capped with reflection free, CO_2 ice. This is apparent in optical imagery (Figs. 4b and X' of 5b inset). On the surface at these locations (Between X' and B) no sublimation features are found, leaving smoother ice than at nearby locations.

Another observation shows that Swiss cheese terrain is frequently found adjacent to the deepest part of a trough on the low side (corresponding to where trough clouds appear) (Figs. 4b, c, 5 and 14). Thomas et al. (2005) mapped the distribution of Swiss cheese terrain but did not discuss the spatial connection (see red points in Fig. 4 from that paper).

The reflection-free zones, discussed by Phillips et al. (2011), are not entirely devoid of reflections. Within the highest troughs, two bright, parallel reflectors trace former surfaces. Utilizing these reflectors, it is possible to constrain the accumulation and migration patterns of these troughs. First, the internal reflectors demonstrate that the deposits comprising reflection free zones and CO_2 ice are not uniform in thickness. They are thickest directly over the former trough bottom and thin toward the trough low side – qualitatively the same as was found on NPLD troughs (Smith and Holt, 2010).

Second, reflections clearly indicate that the current location of the major troughs is closer to the pole than the reflector directly below it (arrows in Fig. 5d). The highest trough in this observation has migrated >16 km during the accumulation of ~750 m of ice. The next trough migrated >8 km during deposition of ~310 m. These numbers correspond to 220 and 260 m of migration, respectively, during deposition of 10 m of ice, significantly more migration than NPLD troughs, which have migrated 70–115 m during accumulation of 10 m (Smith and Holt, 2010, in preparation). The major difference between these troughs and NPLD troughs is that their accumulation occurred post trough formation, but troughs of the NPLD developed concurrent to migration.

7. Discussion

7.1. Spiral troughs

The SPLD spiral troughs are much more diverse than those on the NPLD. They range from symmetric and deep in Promethei Lingula to highly asymmetric, on Australe Lingula, to mostly buried in Australe Mensa. In spite of this diversity, and in contrast to troughs on the NPLD, no evidence exists that any SPLD trough formed during a constructional or depositional period. Layered high sides are present for all SPLD troughs. As detected by SHARAD, on the low sides, frequent evidence exists for accumulation and migration, but that accumulation only drapes preexisting topography (Figs. 5, 11, 12 and 13). The presence of purely erosional troughs has been known for some time (Kolb and Tanaka, 2006), but the formation mechanism for the spatially
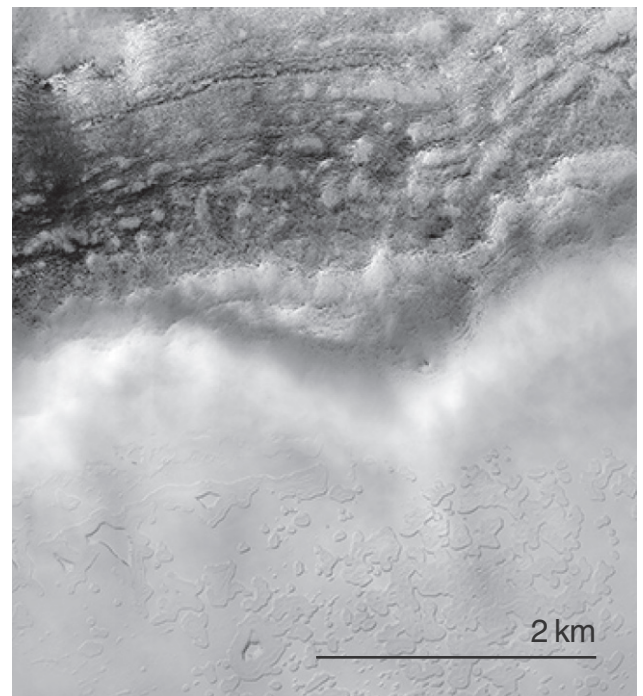
Fig. 14. HiRISE image ESP_031232_0945 capturing Australe Mensa (Region 4) trough cloud. Like in other images, cloud is found near Swiss cheese terrain. With sufficient statistics, clouds become highly predictable and can be targeted with HiRISE.

periodic erosion was not well developed until a cyclic step model was proposed (Smith et al., 2013).

We find that even though they exhibit diversity across several regions, SPLD spiral troughs all fall within the category of features called erosional cyclic steps and are the result of repeating katabatic jumps (sometimes visible as trough clouds). Formerly, the SPLD was much smoother, so trough diversity arises from differences in the underlying substrate that was eroded and subsequent accumulation. In particular, troughs in Australe Mensa formed asymmetrically within the resistive Bench Forming Layers detected by Milkovich and Plaut (2008). Troughs at lower latitudes, in Promethei and Australe Lingula, formed within the Promethei Lingula Layers, which are slope-forming. There, the troughs became deeper, broader, and more symmetric (Fig. 15 left).

In comparison to northern constructional troughs, the erosional cyclic steps of the south likely formed when water vapor was less abundant disallowing deposition on the low side (Fig. 15 left). Nevertheless, katabatic jumps are still a necessary requirement for cyclic steps, so winds must have been sufficiently fast for them to form. Because the SPLD troughs are significantly older than NPLD troughs (based on crater counting of the surface), and likely older than all of the NPLD, they indicate that conditions were favorable for troughs to form at another time.

It was only after formation (potentially much later based on crater counts) that Promethei Lingula troughs and those at the lowest latitude Australe Lingula began to diverge. Whereas Australe Lingula troughs accumulated ice on the low sides and inter-trough regions (Fig. 15 right), Promethei Lingula troughs received very little accumulation. Finally, Australe Mensa troughs, which initially matched those at the highest latitudes in Australe Lingula, received even more accumulation. We find troughs that migrated very quickly to reach the current shape and location after the trough forming erosion.

7.2. Cloud seasonality

Of primary importance in understanding SPLD surface processes are the trough clouds. Trough clouds indicate a high degree of atmospheric activity near the pole, especially strong winds, transport of ice, upstream sublimation, and local deposition. Clouds form within several regions on the SPLD at increasingly higher latitudes as the season changes from early spring until mid-summer, demonstrating that the atmosphere above and near the SPLD experiences significant variability throughout the year. To form clouds, the proper conditions must be met regarding pressure, temperature, and vapor saturation. Therefore, the changing
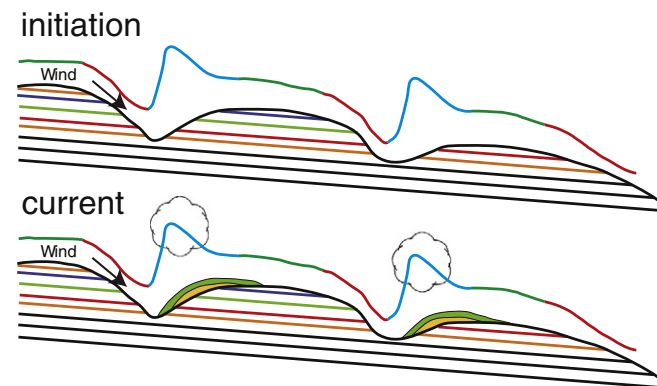
Fig. 15. Cartoon depiction of SPLD trough development. Top: troughs were cut into existing deposits as cycle steps, leaving layered terrain on both sides. Katabatic jumps are required to form the cycle, but water vapor was insufficient for clouds to form, and no material was deposited on the trough low side. Bottom: When conditions became favorable for trough clouds to form, deposition in Australe Lingula and Australe Mensa fully or partially infilled the troughs. Troughs in Promethei Lingula are closer to their initiation state than elsewhere on the SPLD.

seasons affect more than temperature; it affects the deposition and retention of ice on the pole during warm months.

Smith et al. (2013) found that trough clouds are the result of katabatic jumps, or rapid changes in flow properties of strong katabatic winds. Locations with the strongest winds are more likely to exhibit trough clouds. We find a strong agreement between where fast winds are modeled and the locations of trough clouds (Fig. 8). Our simulations suggest that the fastest winds are found in the vicinity of the seasonal CO_2 ice crocus line, especially when topography is present to accelerate slope winds. As the seasonal frost retreats toward the pole, so do the fastest winds and trough clouds.

Clouds are not found everywhere that fast winds are modeled, however. In these cases, katabatic jumps are still likely to form, but an optically thick cloud is not present because insufficient water vapor is available. For example CO_2 seasonal frost covers much of the polar cap in early spring, and only the lowest latitudes are defrosted. This is where clouds are detected (Fig. 8t1). Locations fully covered with CO_2 exhibit no clouds.

This relationship is not without exceptions. Enhanced sublimation on trough high sides (where insolation and warming from wind are greatest) can expose underlying water ice before the crocus line reaches that latitude. This is evident in Fig. 4a, where water ice layers are visible on the high side, but the crocus line has not reached that latitude (Fig. 8m2). Water ice, once exposed, may sublime and offer the necessary vapor to form a cloud (if katabatic jumps are present). Future work will concentrate on individual troughs to test this hypothesis.

Clouds are not detected on the SPLD after L_s 318° (Fig. 8m4). Because water ice is abundant on the surface and surface slopes have changed only minutely, another factor must be important. Temperature contrasts, responsible for fast winds near the poles, are minimal (Fig. 8t4) and responsible for the lack of katabatic jumps.

Relative to the NPLD, Region 4 clouds manifest well beyond the expected date range into mid-summer. Except for a few clouds detected at the SPLD margin, Region 4 clouds appear later than all other SPLD trough clouds (Figs. 6f and 9). In their initial survey of SPLD trough clouds, Smith et al. (2013) suggested that the formation and timing of Region 4 clouds might be related to CO_2 properties. This offers two plausible explanations for the late occurrence of Region 4 clouds. First, as discussed above, water vapor is likely not available in sufficient quantities early in the season. In this case, the troughs are defrosted later in the season. An enduring residual CO_2 cap creates strong thermal contrast, permitting fast winds and the late L_s appearance of clouds.

Also plausible, Region 4 trough clouds may be composed of CO_2 ice rather than water ice. Certainly sufficient CO_2 gas exists in the atmosphere, and nearby CO_2 ice on the surface suggests that stability is possible, but the thermal and pressure requirements to form CO_2 ice in the atmosphere may not be met within katabatic jumps. Also detracting from this idea is that abundant wind speeds and CO_2 vapor are present earlier in the season, but no clouds form at that time (Fig. 8t1 and t2). CO_2 ice clouds should be present then, when temperature and pressure conditions are more favorable. This question cannot be answered without a more detailed investigation including spectral analysis of Region 4 clouds and higher resolution atmospheric simulations.

Region 3 also provides an enigma. Clouds are detected in 5 THEMIS VIS images here early in the season, from L_s 198° to 220°. The clouds are then completely absent for more than 20° L_s and return in abundance after L_s 240°. Whereas the early clouds are few, this observation provokes more questions about water vapor availability and wind speeds. It is possible that the temporal separation of cloud detections in Region 3 results from uneven sampling; however, we believe this phenomenon to be real. Coverage of Region 3 is poor in some years (MY 28–31); however, coverage is very healthy in MY26 and MY27 and in previous years with MOC data. Each has the same observed relationship.

Our examination of THEMIS images over six Mars years and an ongoing analysis using MOC data provides ample imagery to study the

presences of clouds. We find that the clouds are perennial south polar features in the current epoch and expect that future surveys will be able to use these results for predicting the locations of trough clouds. In fact, we were able to successfully target several clouds with HiRISE in Mars Year 31 from predictions based on the THEMIS survey (Fig. 14 and others not shown here ESP_031048_0945, ESP_031100_0945).

7.3. Cloud correspondence to accumulation

Smith et al. (2013) found that trough clouds are a sign of interaction between the atmosphere and surface, i.e. clouds indicate the sites of deposition and ice retention. This relationship means that locations with few or no cloud detections receive little deposition, whereas locations with abundant clouds should have strong evidence of accumulation. We find this to be true on the SPLD as well. SHARAD detects recent accumulation (deposition post trough incision) in Australe Lingula and Australe Mensa, where trough clouds are abundant (Figs. 5 and 12). In contrast, no trough clouds have been detected in the majority of Promethei Lingula, nor has significant recent accumulation been detected there (Fig. 11). The resulting conclusion is that trough morphology, through deposition at trough clouds and katabatic jumps, is the result of seasonal processes directly related to the retreat of the SPLD seasonal CO_2.

7.4. Relation to southern dust storms

A previous study has used Martian mesoscale modeling to simulate dust lifting at the South Pole of Mars (Toigo et al., 2002). This study found that the CO_2 seasonal cap edge was the primary control on enhanced winds, describing "sea breeze" like conditions. Toigo et al. (2002) found that as the southern spring progressed and seasonal cap retreated, the area of sufficiently fast winds also retreated, creating the seasonal, polar dust storm (Martin et al., 1992). Additionally, topographic slopes were determined to be secondary to the ground temperature in enhancing winds. This is in good agreement with our simulations, but those were completed with lower spatial resolution and at only three dates: L_s 225°, 255°, and 310°. Further investigations with our simulations may provide more insight into the annual south polar dust storm and increased dust activity near the crocus line at other times.

7.5. Secondary SPLD morphologies

Various secondary features are of interest on the SPLD. They include minor troughs of the SRIC and Swiss cheese terrain. These features are not ubiquitous; both the immature troughs and the Swiss cheese belong to the residual CO_2 ice cap and the AA_3 unit (Thomas et al., 2005; Phillips et al., 2011). Therefore, they are most likely created by local processes. Because insolation is mostly a uniform forcing, and because deposition is generally smooth, we favor an interpretation of local winds influencing the formation of these features through sublimation. Being within or between troughs, these secondary features must form on relatively short time scales. For example, it was only after infill of A_A3 that the minor troughs took the current shape (Fig. 5). They must, then, be the result of recent atmospheric processes, perhaps indications of short term climate.

Minor troughs have short wavelengths and penetrate only a few tens of meters into the RFZ_3 unit (Figs. 4 and 5). There is no direct correlation between these features and troughs on the NPLD can be made, but minor trough dimensions and locations between troughs are reminiscent of the NPLD undulations (Cutts et al., 1979; Howard, 2000). Recent work has suggested that NPLD undulations are similar to Antarctic megadunes, or aeolian antidunes (Herny et al., 2014), and Smith et al. (2013) modeled Froude numbers close to the range required for antidunes (0.9–1.5) in that region. The presence of undular clouds near nearby south polar troughs (Fig. 5) is a strong indication of similar

Froude numbers near the minor troughs. We hypothesize, then, that the minor troughs on the SPLD formed as a result of flow properties similar to the NPLD undulations, except perhaps in an environment of sublimation rather than deposition.

We observe that Swiss cheese structures are frequently found near to where clouds are detected in Region 4, on the low sides of spiral troughs (Figs. 4, 5, and 14). This association is not likely to be a coincidence, and three factors may contribute to the correspondence, each helping to preserve the CO_2 longer than in surrounding regions. First, the trough low sides slope toward the pole. This geometry favors reduced insolation during the warmest part of the day. In comparison, nearby trough high sides (mostly equator facing slopes) and inter-trough regions (with minimal slopes) are exposed to more direct sunlight at local noon.

The other two factors relate to trough clouds, which are always found near trough low sides. Optically thick clouds reduce insolation at the surface, protecting the thin deposits that contain swiss cheese. Further protection comes from the lower temperature associated with the downstream side of katabatic jumps (Lied, 1964), increasing the stability of surface CO_2. With these protections, the formerly more extensive deposit may sublime more slowly, leaving Swiss cheese pits. These cases are not mutually exclusive, and all three complement each other to preserve Swiss cheese terrain longer than in surrounding regions. A possibility exists, although unlikely, that the clouds themselves are made up of CO_2 and are, therefore, depositing (or have deposited) CO_2 ice on trough low sides prior to Swiss cheese sublimation.

8. Conclusions

Previous south polar studies have been limited to surface exposures and topography. To offer more insight into processes affecting relevant features, we include observations from above the surface in the form of low altitude clouds, indicating the presence of katabatic jumps, and mesoscale modeling. Furthermore, using SHARAD, we have detected subsurface stratigraphy that is relevant to past accumulation, modeled wind patterns, and the location of trough clouds indicating current deposition.

We find that, unlike the NPLD, all of the SPLD troughs initially formed during erosion. Repeated katabatic jumps, in a cyclic step pattern, removed ice at wavelengths determined by regional slope and other factors, eventually forming the troughs. Katabatic winds, driven by pressure contrasts and deflected by the Coriolis force, determined initial orientation of the katabatic jumps (perpendicular to the wind vectors). Based on crater dating and stratigraphic evidence, the troughs were likely in place for timescales of 10^6–10^7 years before significant changes were made in their history (Herkenhoff and Plaut, 2000; Koutnik et al., 2002). During this time they grew in depth and width, with trough morphologies depending on the initial substrate.

After the troughs underwent this expansion, katabatic winds transported ice (via clouds) to troughs in Australe Mensa and Australe Lingula. At the same time, Promethei Lingula troughs continued eroding (Fig. 15 right and left, respectively). Troughs in Australe Mensa have accumulated as much as 700 m of CO_2 ice on the low sides. On Australe Lingula measurable accumulation is detected from after trough formation. Low sides accumulated very little while the inter-trough deposits reach thicknesses of 140 m.

Our mesoscale atmospheric simulations demonstrate that winds are very fast near the boundary between the seasonal CO_2 crocus line and the exposed, underlying, permanent ice cap. As this crocus line retreats poleward during spring and summer, so do the fast winds. Where the winds are fastest and water vapor availability is high, katabatic jumps (and trough clouds) are expected to form. Our observations of cloud appearances match well with the location of the crocus line and fastest winds.

Clouds play an important role in determining where accumulation will occur. Locations where clouds are not observed, Promethei Lingula

and western Australe Scopuli, correspond to those where the oldest SPLD unit, Aa_1, is exposed on the surface (Tanaka et al., 2007). Regions with frequent clouds, Australe Mensa and Australe Lingula, coincide with where younger deposits (AA_2 and AA_3) are thickest. Thus the clouds indicate sites of deposition and retention of ice. In this way, clouds locations influenced by the retreating CO_2 seasonal cap tell us where annual and long-term accumulation occurs. Thus, it is possible, and eventually testable with adequate modeling, that trough morphology is interdependent on a seasonal CO_2 ice cap and that the troughs themselves may require a seasonal cap to initiate.

References

Brothers, T.C., Holt, J.W., Spiga, A., 2013. Orbital radar, imagery, and atmospheric modeling reveal an aeolian origin for Abalos Mensa, Mars. Geophys. Res. Lett. http://dx.doi.org/10.1002/grl.50293 (n/a–n/a).

Byrne, S., 2009. The polar deposits of Mars. Annu. Rev. Earth Planet. Sci. 37 (1), 535–560. http://dx.doi.org/10.1146/annurev.earth.031208.100101.

Byrne, S., Ingersoll, A.P., 2003. A Sublimation Model for Martian South Polar Ice Features, p. 5609.

Byrne, S., Ivanov, A.B., 2004. Internal structure of the Martian south polar layered deposits. J. Geophys. Res. Planets 109 (E11). http://dx.doi.org/10.1029/2004JE002267 (n/a–n/a).

Campbell, B.A., Putzig, N.E., Carter, L.M., Phillips, R.J., 2011. Autofocus correction of phase distortion effects on SHARAD echoes. IEEE Geosci. Remote Sens. Lett. 8 (5), 939–942. http://dx.doi.org/10.1109/LGRS.2011.2143692.

Cantor, B.A., James, P.B., Caplinger, M., Wolff, M.J., 2001. Martian dust storms: 1999 Mars Orbiter Camera observations. J. Geophys. Res. 106, 23653–23688. http://dx.doi.org/10.1029/2000JE001310.

Christensen, P.R., et al., 2004. The Thermal Emission Imaging System (THEMIS) for the Mars 2001 Odyssey mission. Space Sci. Rev. 110 (1/2), 85–130. http://dx.doi.org/10.1023/B:SPAC.0000021008.16305.94.

Clifford, S.M., 1987. Polar basal melting on Mars. J. Geophys. Res. 92 (B9), 9135–9152.

Cutts, J.A., 1973. Wind erosion in the Martian polar region. J. Geophys. Res. 78.

Cutts, J., Blasius, K., Roberts, W., 1979. Evolution of Martian polar landscapes—Interplay of long-term variations in perennial ice cover and dust storm intensity. J. Geophys. Res. 84 (B6), 2975–2994.

Farmer, C.B., Doms, P.E., 1979. Global seasonal variation of water vapor on Mars and the implications for permafrost. J. Geophys. Res. Solid Earth 84 (B6), 2881–2888. http://dx.doi.org/10.1029/JB084iB06p02881.

Farrell, W.M., et al., 2008. MARSIS subsurface radar investigations of the South Polar reentrant Chasma Australe. J. Geophys. Res. Planets 113 (E4). http://dx.doi.org/10.1029/2007JE002974 (n/a–n/a).

Fishbaugh, K.E., Head III, J.W., 2001. Comparison of the North and South Polar caps of Mars: new observations from MOLA data and discussion of some outstanding questions. Icarus 154 (1), 145–161. http://dx.doi.org/10.1006/icar.2001.6666.

Fishbaugh, K.E., Head III, J.W., 2002. Chasma Boreale, Mars: topographic characterization from Mars Orbiter Laser Altimeter data and implications for mechanisms of formation. J. Geophys. Res. 107 (E3), 5013.

Fishbaugh, K.E., Byrne, S., Herkenhoff, K.E., Kirk, R.L., Fortezzo, C., Russell, P.S., McEwen, A., 2010. Evaluating the meaning of "layer" in the Martian north polar layered deposits and the impact on the climate connection. Icarus 205, 269–282. http://dx.doi.org/10.1016/j.icarus.2009.04.011.

Fisher, D.A., 1993. If Martian ice caps flow: ablation mechanisms and appearance. Icarus 105 (2), 501–511.

Fisher, D.A., 2000. Internal layers in an "accublation" ice cap: a test for flow. Icarus 144 (2), 289–294.

Grima, C., Kofman, W., Mouginot, J., Phillips, R.J., Hérique, A., Biccari, D., Seu, R., Cutigni, M., 2009. North polar deposits of Mars: extreme purity of the water ice. Geophys. Res. Lett. 36 (3), L03203.

Grima, C., Costard, F., Kofman, W., Saint-Bézar, B., Servain, A., Rémy, F., Mouginot, J., Herique, A., Seu, R., 2011. Large asymmetric polar scarps on Planum Australe, Mars: characterization and evolution. Icarus 212 (1), 96–109. http://dx.doi.org/10.1016/j.icarus.2010.12.017.

Herkenhoff, K., Plaut, J.G., 2000. Surface ages and resurfacing rates of the polar layered deposits on Mars. Icarus 144 (2), 243–253. http://dx.doi.org/10.1006/icar.1999.6287.

Herny, C., Massé, M., Bourgeois, O., Carpy, S., Le Mouélic, S., Appéré, T., Smith, I.B., Spiga, A., Rodriguez, S., 2014. Sedimentation waves on the Martian North Polar Cap: analogy with megadunes in Antarctica. Earth Planet. Sci. Lett. 403, 56–66.

Holt, J.W., Peters, M.E., Kempf, S.D., Morse, D.L., Blankenship, D.D., 2006. Echo source discrimination in single-pass airborne radar sounding data from the Dry Valleys, Antarctica: implications for orbital sounding of Mars. J. Geophys. Res. Planets 111 (E6), E06S24.

Holt, J.W., Fishbaugh, K.E., Byrne, S., Christian, S., Tanaka, K., Russell, P.S., Herkenhoff, K.E., Safaeinili, A., Putzig, N.E., Phillips, R.J., 2010. The construction of Chasma Boreale on Mars. Nature 465 (7297), 446–449. http://dx.doi.org/10.1038/nature09050.

Howard, A.D., 2000. The role of Eolian processes in forming surface features of the Martian polar layered deposits. Icarus 144 (2), 267–288.

Howard, A.D., Cutts, J.A., Blasius, K.R., 1982. Stratigraphic relationships within Martian polar cap deposits. Icarus 50 (2–3), 161–215.

Hvidberg, C.S., Fishbaugh, K.E., Winstrup, M., Svensson, A., Byrne, S., Herkenhoff, K.E., 2012. Reading the climate record of the Martian polar layered deposits. Icarus 221 (1), 405–419. http://dx.doi.org/10.1016/j.icarus.2012.08.009.

Kauhanen, J., Siili, T., Järvenoja, S., Savijärvi, H., 2008. The Mars limited area model and simulations of atmospheric circulations for the Phoenix landing area and season of operation. J. Geophys. Res. Planets 113. http://dx.doi.org/10.1029/2007JE003011.

Kieffer, H.H., 1979. Mars south polar spring and summer temperatures: a residual CO_2 frost. J. Geophys. Res. Solid Earth 84 (B14), 8263–8288. http://dx.doi.org/10.1029/JB084iB14p08263.

Kieffer, H.H., Titus, T.N., 2001. TES mapping of Mars' north seasonal cap. Icarus 154 (1), 162–180. http://dx.doi.org/10.1006/icar.2001.6670.

Kieffer, H.H., Titus, T.N., Mullins, K.F., Christensen, P.R., 2000. Mars south polar spring and summer behavior observed by TES: seasonal cap evolution controlled by frost grain size. J. Geophys. Res. Planets 105 (E4), 9653–9699. http://dx.doi.org/10.1029/1999JE001136.

Kolb, E.J., Tanaka, K.L., 2001. Geologic history of the polar regions of mars based on mars global surveyor data II. Amazonian Period. Icarus 154 (1), 22–39.

Kolb, E.J., Tanaka, K.L., 2006. Accumulation and erosion of south polar layered deposits in the Promethei Lingula region, Planum Australe, Mars. Int. J. Mars Sci. Explor. 2, 1–9.

Kostic, S., Sequeiros, O., Spinewine, B., Parker, G., 2010. Cyclic steps: a phenomenon of supercritical shallow flow from the high mountains to the bottom of the ocean. J. Hydro Environ. Res. 3 (4), 167–172.

Koutnik, M., Byrne, S., Murray, B., 2002. South polar layered deposits of Mars: the cratering record. J. Geophys. Res. 107, 5100.

Koutnik, M.R., Byrne, S., Murray, B.C., Toigo, A.D., Crawford, Z.A., 2005. Eolian controlled modification of the Martian south polar layered deposits. Icarus 174 (2), 490–501. http://dx.doi.org/10.1016/j.icarus.2004.09.015.

Levrard, B., Forget, F., Montmessin, F., Laskar, J., 2007. Recent formation and evolution of northern Martian polar layered deposits as inferred from a global climate model. J. Geophys. Res. 112 (E6), E06012.

Lied, N.T., 1964. Stationary hydraulic jumps in a katabatic flow near Davis, Antarctica, 1961. Aust. Meteorol. Mag. 47, 40–51.

Malin, M.C., et al., 1998. Early views of the Martian surface from the Mars Orbiter Camera of Mars global surveyor. Science 279 (5357), 1681–1685. http://dx.doi.org/10.1126/science.279.5357.1681.

Malin, M.C., et al., 2007. Context camera investigation on board the Mars Reconnaissance Orbiter. J. Geophys. Res. Planets 112 (E5). http://dx.doi.org/10.1029/2006JE002808 (n/a–n/a).

Martin, L.J., James, P.B., Clancy, T.R., Lee, S.W., Kahn, R.A., Zurek, R.P., Singer, R.B., 1992. Hubble Space Telescope observations of Martian clouds, hazes, and polar caps during cycle I. Bulletin of the American Astronomical Society vol. 24, p. 1007.

Massé, M., Bourgeois, O., Le Mouélic, S., Verpoorter, C., Spiga, A., Le Deit, L., 2012. Wide distribution and glacial origin of polar gypsum on Mars. Earth Planet. Sci. Lett. 317–318, 44–55. http://dx.doi.org/10.1016/j.epsl.2011.11.035.

McEwen, A.S., Eliason, E.M., Bergstrom, J.W., Bridges, N.T., Hansen, C.J., Delamere, W.A., Grant, J.A., Gulick, V.C., Herkenhoff, K.E., Keszthelyi, L., 2007. Mars Reconnaissance Orbiter's high resolution imaging science experiment (HiRISE). J. Geophys. Res. Planets 112 (E5).

Milkovich, S.M., Plaut, J.J., 2008. Martian south polar layered deposit stratigraphy and implications for accumulation history. J. Geophys. Res. Planets 113 (E6), E06007.

Montmessin, F., Forget, F., Rannou, P., Cabane, M., Haberle, R.M., 2004. Origin and role of water ice clouds in the Martian water cycle as inferred from a general circulation model. J. Geophys. Res. 109 (E10), E10004. http://dx.doi.org/10.1029/2004JE002284.

Murray, B., Koutnik, M., Byrne, S., Soderblom, L., Herkenhoff, K., Tanaka, K.L., 2001. Preliminary geological assessment of the northern edge of Ultimi Lobe, Mars south polar layered deposits. Icarus 154 (1), 80–97.

Neugebauer, G., Münch, G., Kieffer, H., Chase, S.C., Miner, E., 1971. Mariner 1969 infrared radiometer results: temperatures and thermal properties of the Martian surface. Astron. J. 76, 719.

Neukum, G., Jaumann, R., 2004. HRSC: the High Resolution Stereo Camera of Mars Express. Mars Express Sci. Payload 1240, 17–35.

Parker, G., 1996. Some speculations on the relation between channel morphology and channel-scale flow structures. Coherent Flow Structures in Open Channels, pp. 429–432.

Parker, G., Izumi, N., 2000. Purely erosional cyclic and solitary steps created by flow over a cohesive bed. J. Fluid Mech. 419, 203–238.

Pettré, P., André, J.C., 1991. Surface-pressure change through Loewe's phenomena and katabatic flow jumps—Study of two cases in Adelie Land, Antarctica. J. Atmos. Sci. 48, 557–571.

Phillips, R.J., et al., 2011. Massive CO_2 ice deposits sequestered in the South polar layered deposits of Mars. Science 332 (6031), 838–841. http://dx.doi.org/10.1126/science.1203091.

Plaut, J.J., et al., 2007. Subsurface radar sounding of the south polar layered deposits of Mars. Science 316 (5821), 92–95. http://dx.doi.org/10.1126/science.1139672.

Seu, R., et al., 2007a. Accumulation and erosion of Mars' south polar layered deposits. Science 317 (5845), 1715–1718.

Seu, R., Phillips, R.J., Biccari, D., Orosei, R., Masdea, A., Picardi, G., Safaeinili, A., Campbell, B.A., Plaut, J.J., Marinangeli, L., 2007b. SHARAD sounding radar on the Mars Reconnaissance Orbiter. J. Geophys. Res. 112 (E5), E05S05.

Siili, T., Haberle, R.M., Murphy, J.R., Savijarvi, H., 1999. Modelling of the combined late-winter ice cap edge and slope winds in Mars Hellas and Argyre regions. Planet. Space Sci. 47 (8–9), 951–970. http://dx.doi.org/10.1016/S0032-0633(99)00016-1.

Skamarock, W.C., Klemp, J.B., 2008. A time-split nonhydrostatic atmospheric model for weather research and forecasting applications. J. Comput. Phys. 227 (7), 3465–3485.

Smith, I.B., Holt, J.W., 2010. Onset and migration of spiral troughs on Mars revealed by orbital radar. Nature 465 (7297), 450–453. http://dx.doi.org/10.1038/nature09049.

Smith, I.B., Holt, J.W., 2014n. SHARAD detection of regional spiral trough diversity, (in preparation).

Smith, D.E., Zuber, M.T., Frey, H.V., Garvin, J.B., Head, J.W., Muhleman, D.O., Pettengill, G.H., Phillips, R.J., Solomon, S.C., Zwally, H.J., 2001a. Mars Orbiter Laser Altimeter: experiment summary after the first year of global mapping of Mars. J. Geophys. Res. Planets 106 (E10).

Smith, D.E., Zuber, M.T., Neumann, G.A., 2001b. Seasonal variations of snow depth on Mars. Science 294 (5549), 2141–2146. http://dx.doi.org/10.1126/science.1066556.

Smith, I.B., Holt, J.W., Spiga, A., Howard, A.D., Parker, G., 2013. The spiral troughs of Mars as cyclic steps. J. Geophys. Res. Planets http://dx.doi.org/10.1002/jgre.20142 (n/a–n/a).

Spiga, A., Forget, F., 2009. A new model to simulate the Martian mesoscale and microscale atmospheric circulation: validation and first results. J. Geophys. Res. 114 (E2), E02009. http://dx.doi.org/10.1029/2008JE003242.

Spiga, A., Forget, F., Madeleine, J.-B., Montabone, L., Lewis, S.R., Millour, E., 2011. The impact of Martian mesoscale winds on surface temperature and on the determination of thermal inertia. Icarus 212 (2), 504–519. http://dx.doi.org/10.1016/j.icarus.2011.02.001.

Tanaka, K.L., 2005. Geology and insolation-driven climatic history of Amazonian north polar materials on Mars. Nature 437 (7061), 991–994. http://dx.doi.org/10.1038/nature04065.

Tanaka, K.L, Kolb, E.J., Fortezzo, C., 2007. Recent advances in the stratigraphy of the polar regions of Mars. LPI Contrib. 1353, 3276.

Thomas, P.C., Malin, M.C., James, P.B., Cantor, B.A., Williams, R.M.E., Gierasch, P., 2005. South polar residual cap of Mars: features, stratigraphy, and changes. Icarus 174 (2), 535–559. http://dx.doi.org/10.1016/j.icarus.2004.07.028.

Titus, T.N., 2005. Mars polar cap edges tracked over 3 full Mars years. 36th Annual Lunar and Planetary Science Conference vol. 36, p. 1993.

Toigo, A.D., Richardson, M.I., Wilson, R.J., Wang, H., Ingersoll, A.P., 2002. A first look at dust lifting and dust storms near the south pole of Mars with a mesoscale model. J. Geophys. Res. Planets 107 (E7), 4-1–4-13. http://dx.doi.org/10.1029/2001JE001592.

Tyler, D.J., Barnes, J.R., 2005. A mesoscale model study of summertime atmospheric circulations in the North Polar Region of Mars. J. Geophys. Res. 110 (E6), E06007. http://dx.doi.org/10.1029/2004JE002356.

Whiteway, J.A., et al., 2009. Mars water-ice clouds and precipitation. Science 325 (5936), 68.

Zuber, M.T., Smith, D.E., Solomon, S.C., Abshire, J.B., Afzal, R.S., Aharonson, O., Fishbaugh, K., Ford, P.G., Frey, H.V., Garvin, J.B., 1998. Observations of the North Polar Region of Mars from the Mars Orbiter Laser Altimeter. Science 282 (5396), 2053.